Water Research X 28 (2025) 100319

Contents lists available at ScienceDirect

Water Research X

journal homepage: www.sciencedirect.com/journal/water-research-x

Heterogeneous microstructure induces floatation in high-rate anammox granules

Da Kang [a], Huifeng Lu [b], Tingting Kang [b], Yihan Zhang [a], Zheng Ge [a], Liang Zhang [a,*], Yongzhen Peng [a]

[a] National Engineering Laboratory for Advanced Municipal Wastewater Treatment and Reuse Technology, Department of Environmental Engineering, Beijing University of Technology, PR China
[b] Zhejiang Water Healer Environmental Technology Co., Ltd, Hangzhou, PR China

ARTICLE INFO

Keywords:
Anammox granules
Floatation
Gas release
EPS imaging
N-cycling genes

ABSTRACT

The floatation of anammox granules can be a serious challenge in practical wastewater treatment, as it can deteriorate reactor performance and cause bacterial loss. To deepen the understanding of floatation mechanism, in this study, both the floating (F-AnGS) and settling anammox granules (S-AnGS) from a high-rate anammox reactor were comparatively investigated. F-AnGS demonstrated 1.6 times higher specific anammox activity compared to S-AnGS, but only 65 % of produced gas could be successfully released, as quantified by anaerobic respirometry. In addition to the overall EPS accumulation, F-AnGS exhibited a heterogeneous microstructure distinct from that of S-AnGS, as revealed by 3D X-ray microscopic imaging at the single granule level. The heterogeneous distribution of EPS, which can form a dense surface layer, was the main cause for granule floatation. The heterogeneous microstructure of F-AnGS can reduce the distance between microorganisms and enhance the metabolic interaction between anammox bacteria and heterotrophs. The abundance of community members did not have a significant variation, but the functional genes related to anammox and partial denitrification pathway were significantly increased, indicating the enhanced nitrite loop in F-AnGS. This study proposed new structural insights into mechanism of anammox granule floatation, suggesting the appropriate activity control of granule-based anammox process.

1. Introduction

Anaerobic ammonium oxidation (anammox) process, whereby ammonium is anaerobically oxidized to dinitrogen gas with nitrite as electron acceptor instead of utilizing the external organics, has been well recognized as one of the most cost-effective nitrogen removal techniques in wastewater treatment (Kuenen, 2020; McCarty, 2018). Although the installation of anammox process in wastewater engineering has made great achievements worldwide, its widespread applications still face many challenges, especially the shortage of high-quality seed sludge (Cao et al., 2017; Lackner et al., 2014). As slow-growing microorganisms, the doubling time of anammox bacteria (AnAOB) could extend from 3 to 14 days (Oshiki et al., 2016), leading to prolonged startup times and the operational instability of full-scale reactor (Jin et al., 2012; van der Star et al., 2007). Therefore, how to achieve effective retention of anammox biomass become a key issue to promote process stability. The currently employed biomass retention strategies in anammox-based systems has been critically reviewed including granulation, carrier-dependent biofilm, gel entrapment, and membrane separation (Kosgey et al., 2021).

AnAOB usually live in a communal lifestyle, and the specific anammox activity was only detectable when the free-living cell densities higher than 10^7 cells/mL (Oshiki et al., 2020). Moreover, AnAOB are well known for their superior EPS secretion ability, which favors the cell aggregation to form attached biofilms or granules (Ali et al., 2018; Hou et al., 2015; Jia et al., 2017). Microbial self-immobilization to form the dense granular sludge has been proposed as the most promising and cost-saving biotechnology without the addition of carriers or any other extra separation equipment (Adams et al., 2022; Winkler et al., 2018). The average N-load of granule-based partial nitritation/anammox (PN/A) system is about three times higher than other configurations (e.g., SBR, MBBR and others) (Lackner et al., 2014). The first full-scale anammox process in Rotterdam used the granular sludge system and reached the maximum nitrogen conversion rate of 9.5 kg N/(m^3·d)

* Corresponding author.
E-mail address: zliang@bjut.edu.cn (L. Zhang).

https://doi.org/10.1016/j.wroa.2025.100319
Received 17 October 2024; Received in revised form 11 December 2024; Accepted 9 February 2025
Available online 10 February 2025
2589-9147/© 2025 The Authors. Published by Elsevier Ltd. This is an open access article under the CC BY-NC-ND license (http://creativecommons.org/licenses/by-nc-nd/4.0/).

(Abma et al., 2007; van der Star et al., 2007). A super high rate of 74.3–76.7 kg N/(m^3·d) has been reported in the lab-scale anammox up-flow reactor (Tang et al., 2011). Nevertheless, the floatation of anammox granules commonly occurs in practice, especially under high nitrogen loads. Once formed, the anammox granules floating on the liquid surface can be easily washed out of the reactor with the effluent flow, which could even cause the deterioration of reactor performance (Chen et al., 2010).

Previous studies focused on the floatation of anammox granules speculated that the decrease of density by gas pockets formation was the direct reason for the granule floatation. The formation mechanism of gas pockets during the cell granulation process can be summarized into two main aspects: 1) the over-secreted extracellular polymeric substances (EPS) obstructed the gas tunnels around cells (Lu et al., 2012; Xue et al., 2023); 2) the restricted diffusion of substrates caused bacterial starvation, lysis, and form the cavities in the inner zone of granules. A novel diffusion-reaction integrated mathematical model has been proposed and suggested that size was a crucial factor to determine the granule floatation (Tan et al., 2020). However, as three-dimensional micro-aggregates, the determination of size, density, settling velocity, and EPS amount could not reflect the microstructural change within the granule, thus, limiting our knowledge on how settling anammox granules transition to the floating state. Previous study proposed that microbial community composition was not the main reason for sludge flotation since no significant microbial difference between the floated and settled granules (Tao et al., 2020; Song et al., 2017). Xu et al. (2024) demonstrated that dosing folate could weaken the cross-feeding interaction between anammox and other bacteria, thereby reducing EPS secretion and mitigating sludge floatation. However, the microbial mechanism behind granule floatation behavior remains unclear.

In this study, the settling and floating anammox granules from a long-term high-rate anammox reactor were comparatively investigated, in addition to determine the apparent characteristics (specific anammox activity, size, EPS), the anaerobic respirometry was applied to accurately quantify the gas release rate and volume of the floating granules, and the 3D X-ray microscopic imaging was introduced to visualize the *in-situ* spatial microstructure on the single granule level. Furthermore, the anammox communities were analyzed to determine the functional variations. This study provides direct evidence to reveal the microstructural change within granules, and proposes the mechanism for anammox granules shifting between the floating and settling state.

2. Results and discussion

2.1. Floating granules from a stable and efficient anammox reactor

The settling (S-AnGS) and floating anammox granules (F-AnGS) in this study were sampled from a stable and efficient anammox granular system (Fig. S1). The anammox reactor has been operated for over 200 days with the average influent concentrations of ammonium and nitrite as 96.5 ± 20.9 and 135.0 ± 24.4 mg N/L, respectively (Fig. 1a). The effluent concentrations of ammonium and nitrite were 2.9 ± 5.3 and 3.6 ± 5.0 mg N/L (>97 % removal efficiency), and the removal efficiency of total inorganic nitrogen (TIC) was 79.3 ± 7.2 %. The nitrogen removal rate was 1.6 ± 0.4 kg N/(m^3·d) (Fig. 1b). The stoichiometric ratios of nitrite/nitrate to ammonium were in agreement with the typical

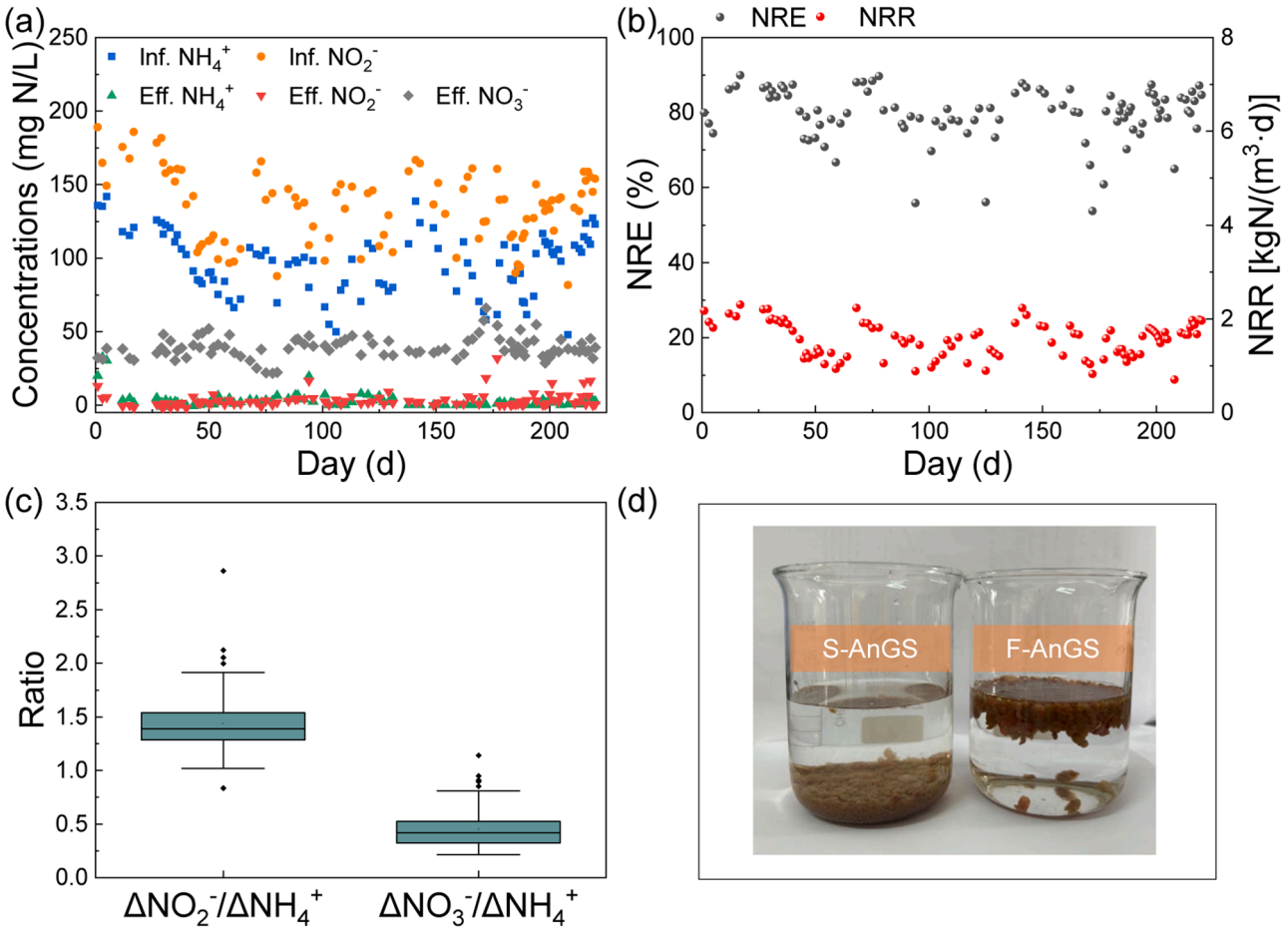

Fig. 1. Long-term performance of anammox granular system. (a) concentrations of influent and effluent nitrogenous compounds; (b) nitrogen removal efficiency (NRE) and nitrogen removal rate (NRR); (c) stoichiometric ratios of nitrogenous compounds; (d) images of the settling (S-AnGS) and floating anammox granules (F-AnGS) used in this study.

anammox reaction (Fig. 1c) (Lotti et al., 2014; Strous et al., 1998). During the operation period, there was a consistent accumulation of floating granules on the liquid surface, which were collected to compare with the normal settling granules at the bottom of the reactor (Fig. 1d).

2.2. Gas entrapment in floating granules with increased specific activity

Since anammox process converts ammonium and nitrite to form nitrogen gas, the specific anammox activity (SAA) of anammox aggregates could be characterized by both substrate consumption rate or gas production rate (van Loosdrecht et al., 2016). The batch tests showed typical nitrogen profiles of the anammox reaction (concurrent consumption of ammonium and nitrite with nitrate production, Fig. S2) and surprisingly, F-AnGS exhibited a significantly higher SAA at 68.4 ± 3.7 (mg N/g VSS·d) than S-AnGS at 42.6 ± 1.9 (mg N/g VSS·d) ($p < 0.01$) (Fig. 2a), indicating the flotation behavior was not caused by activity deterioration, and highlighting the necessity to retain the high-rate floating anammox granules.

The granule floatation was thought to be caused by the restricted gas release (Chen et al., 2010). Furthermore, we used the anaerobic respirometry to quantify the gas release volume and rate during the batch activity tests. When the cumulative gas volume curve levelled off, the fresh substrate was injected into the vessels and three consecutive cycles were repeated. In contrast to the substrate consumption rate, the respirometric results showed that the maximum gas production rate of S-AnGS (1.85 ± 0.40 mL/(g·d)) was higher than that of F-AnGS (1.41 ± 0.02 mL/(g·d)), and the maximum gas accumulation volume of S-AnGS could reach 19.1 ± 0.5 mL, which was close to the theoretical stoichiometric value, but for F-AnGS, only ~65 % gas could be successfully released (12.2 ± 0.5 mL in total) (Fig. 2b). These results quantitively demonstrated the previous assumption that the accumulation of gas inside would decrease the density of granules and finally lead to the sludge floatation (Lu et al., 2012; Xue et al., 2023). Previous study proposed that the specific anammox activity could be measured by headspace pressure variation (Dapena-Mora et al., 2007), but it should be aware that the type or size may largely impact the gas entrapment ability, which would bias the activity, especially for the dense granules.

2.3. Size, composition and abundance of EPS

The granular sludge, as self-immobilized microbial aggregates, consists of densely packed microorganisms, EPS, gas-liquid channels, and inorganic particles. The size and EPS component analysis are the commonly used methods to characterize the granular sludge. The size of granular sludge not only determines its settling velocity (Lu et al., 2013), but also affects its mass transfer efficiency (Zhu et al., 2018). Anammox granules are found to exhibit a wide size distribution, ranging from 0.5 mm to 4.0 mm (Ni et al., 2009). The size distribution curve showed that both F-AnGS and S-AnGS were composed of flocs (<0.5 mm, 43.3–44.4 % v/v) and granules (>0.5 mm, 55.6–56.7 % v/v) (Fig. 3a). The Volume Mean Diameter (VMD) of F-AnGS was 737.7 μm larger than S-AnGS at 667.3 μm. This result aligns with previous studies, which indicate that larger granule sizes do not necessarily lead to better performance. The optimal granule size was identified as 0.5–0.9 mm, striking a balance between efficient mass transfer and sustained microbial activity (Xu et al., 2021; Zhu et al., 2018). Furthermore, a higher proportion of large granules (1.0–2.0 mm) was observed in F-AnGS compared to S-AnGS (30.2 % vs. 20.3 %), indicating the significant volumetric expansion for the floating granules.

The self-produced extracellular polymeric substances (EPS) play a key role in immobilizing cells in close proximity and the over-secretion of EPS was thought to be the main reason for blocking the gas-liquid channel and causing the sludge floatation (Song et al., 2017). Organic matters in EPS include polysaccharides (PS), proteins (PN), humic acids (HA), nucleic acids, and other biopolymers (Flemming and Wingender, 2010). Herein, the EPS component analysis showed that PN, compared to PS, was the predominant component in all three EPS subfractions, and the PN content of F-EPS was significantly higher than S-EPS (458.7 ± 2.3 mg/g VSS vs. 103.4 ± 13.9 mg/g VSS, $p < 0.01$) (Fig. 3b). PNs include both enzymes and structural proteins, which are highly related to microbial metabolism, intercellular communication, and biofilm formation. Some enzymes can degrade EPS to provide energy and carbon sources for cells, while other enzymes can promote cell attachment and detachment. The non-enzymatic proteins may help maintain structural integrity by interacting with other EPS components like polysaccharides and nucleic acids (Xiao et al., 2016; Yu et al., 2023).

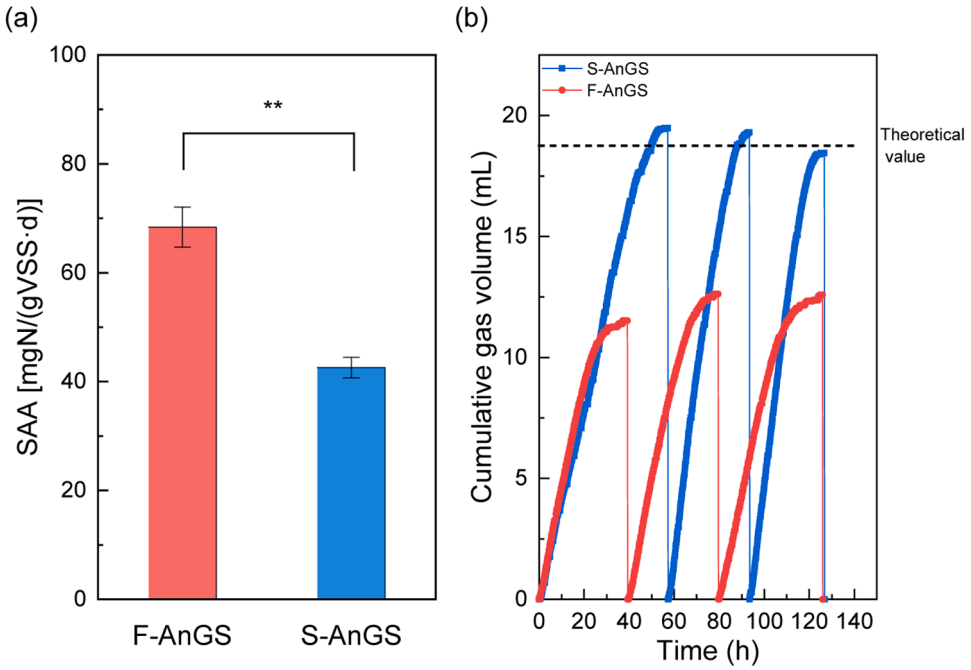

Fig. 2. Specific anammox activity (SAA) of S-AnGS and F-AnGS as determined by substrate consumption rate (a) and on-line gas monitoring (b) using batch activity test.

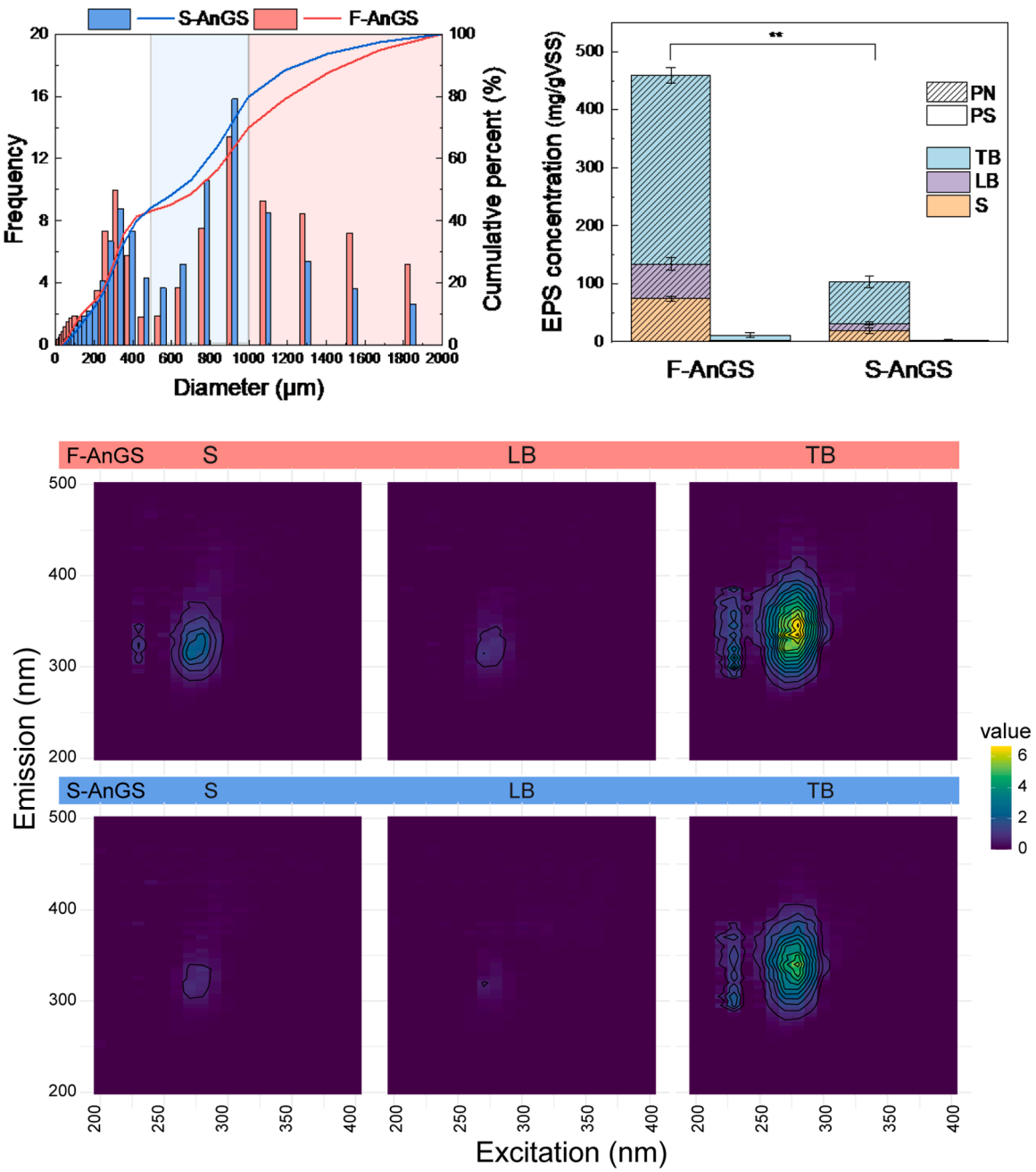

Fig. 3. Particle size distribution (a), concentration of proteins (PN) and polysaccharides (PS) (b), and fluorescence analysis of stratified EPS (S-slime; LB-loosely bound EPS; TB-tightly bound EPS) (c).

Furthermore, EPS exhibits a stratified structure containing tightly-bound EPS (TB-EPS), loosely-bound EPS (LB-EPS), and soluble EPS (S-EPS). The PN and PS were found to vary across the TB-/LB-/S-EPS. Specifically, PN had the highest percentage in the TB-EPS layer ranging from 67.0 % to 74.9 %, while the LB-EPS layer contained the lowest PN content, varying between 8.3 % and 17.2 %. This suggests that AnGS had a stronger aggregation ability of cells than the further flocculation ability of flocs. Moreover, the 3D-EEM analysis revealed that TB-EPS layer had the strongest fluorescence intensities compared to the S and LB layers, and 8 peaks could be identified in total according to the previous literature (Chen et al., 2003) (Table S3). Most of the peaks (Peak 4–8) belonged to soluble microbial by-product-like Region IV at Em/Ex of (335–345)/(260–300) nm, which are described as tryptophan-related biological process. Other peaks (Peak 1–3) were ascribed to Aromatic protein (Region I and II). F-AnGS had the higher tryptophan-like intensity located at Em/Ex of 345/280 nm than S-AnGS (6.59 vs. 5.28) (Fig. 3c), which was consistent with the previous finding that protein-like substance was the most widely distributed substance in all three stratified EPS (Jia et al., 2017). Overall, a large increase of protein-like EPS was observed in the floating granules compared to the settling granules, with no significant compositional differences detected.

2.4. Visualization of the heterogeneous distribution of EPS in floating granules

In addition to the conventional chemical analysis of EPS mentioned above, the three-dimensional (3D) X-ray microscope (XRM) was applied to visualize the microstructure of F-AnGS and S-AnGS, respectively. The XRM provides new insights into microstructure at the single granule level using non-destructive imaging at high-resolution and high

contrast. Approximately 1000 images were captured along the thickness (~3.5 μm) to reveal the cross-section of the single granule. The imaging results clearly showed the cross sections of the EPS predominantly as bright lines. Significantly different distribution patterns of EPS were observed between the single floating granule and the settling granule. For the F-AnGS, EPS was primarily distributed on the surface, forming well-interconnected structures with relatively uniform lengths and thicknesses (Fig. 4a). The center was hollow (marked in yellow circles), with no EPS penetration. In contrast, the internal EPS of S-AnGS exhibited an irregular distribution with varying lengths and thicknesses, and they were not closely interconnected (Fig. 4b). EPS can be distributed in both the inner layer and on the surface, which would favor the rapid gas release from the inside. Furthermore, the raw cross-section images were computationally combined to generate a 3D reconstruction of the granule's volume. The colored 3D data showed a higher density in the surface layer of F-AnGS compared to S-AnGS, and F-AnGS formed more concentrated microaggregates with larger sizes (red dots marked in red circles). In conclusion, this study introduced the advanced XRM imaging technology and confirmed the dense structure within the floating anammox granules, which was consistent with the higher EPS concentration and intensity as determined in Fig. 3. Moreover, we revealed the heterogenous EPS distribution within the floating granules, which could block the gas release channels and subsequently lead to sludge floatation. However, larger microbial aggregates were detected within the floating granules, which could explain the higher specific anammox activity and the higher EPS content detected in F-AnGS.

Previous study has observed the nanobubbles, which can be trapped inside the anammox granules, affecting its density and stability (Fu et al., 2021). The BET technique was used to quantify the surface area, pore volume and pore size distribution of the high-porosity granules using N_2 as the carrier gas. The adsorption-desorption isotherms exhibited typical type III isotherm according to IUPAC classification (Gregg et al., 1967), no flattish portion was found in the curve which indicated no monolayer was formed and the irregular mesopores (between 2 and 50 nm) or macropores (larger than 50 nm) were the dominant pore size inside anammox granules with weak interaction between the adsorbate (N_2) and the adsorbent (biomass) (Fig. 4c). The surface aera and total pore volume of F-AnGS (3.061 m^2/g VSS and 0.01567 cm^3/g VSS) were higher than those of S-AnGS (2.827 m^2/g VSS and 0.01546 cm^3/g VSS), indicating that more N_2 could be accumulated inside the floating granules. Whereas, the average pore diameter of S-AnGS (21.87 nm) was larger than that of F-AnGS (20.47 nm), indicating the produced N_2 bubbles could more easily escape out of S-AnGS compared to F-AnGS. Overall, we demonstrated the microstructural change in the floating anammox granules with heterogeneous EPS distribution.

2.5. Higher abundance of N-cycling genes in floating granules

To investigate the microbial dynamics between F-AnGS and S-AnGS, 16S rRNA gene sequencing was firstly applied to analyze the microbial communities. The results showed that most of ASVs (225, accounting for 93 %−98 %) were overlapped in different samples indicating the microbial taxa between F-AnGS and S-AnGS were highly similar (Fig. S3). S-AnGS had a higher median Simpson index than F-AnGS (0.043 vs. 0.032), indicating the increase of biodiversity when floatation occurred, but no significant difference was examined ($p > 0.05$, Fig. S4). At the genus level, *Candidatus* Brocadia was the most dominant anammox bacteria (AnAOB) in both F-AnGS and S-AnGS varying from 21.3 % to 35.4 %, while *Candidatus* Kuenenia, as another common genus of AnAOB, accounted for only 0.4 % to 1.4 % (Fig. 5a). However, no significant difference of AnAOB abundance was examined between F-AnGS and S-AnGS (Welch's *t*-test, $p > 0.05$). In addition to the anammox bacteria, heterotrophic denitrifiers including Denitratisoma, OLB13, and Ignavibacterium were abundant within the granules. Denitratisoma belong to the phylum Proteobacteria, and were reported to be the main accompanying bacteria in the anammox system and contain functional genes related to partial denitrification (Zhou et al., 2023). OLB13 belong to the phylum Proteobacteria, and had the ability to reduce nitrate and/or nitrite (Xiao et al., 2022). Ignavibacterium are affiliated with the class Ignavibacteria, which appeared to be fermentative anaerobic bacteria and participated in denitrification pathway (Ma et al., 2023). Compared to S-AnGS (14.3 ± 3.8 %), F-AnGS had a higher abundance (18.4 ± 1.1 %) of these potential denitrifying bacteria, which could contribute to the nitrate reduction and enhance the nitrite loop between anammox bacteria and heterotrophs. However, only very few genera (e.g., *Arenimonas*, SWB02, *Limnobacter*, UTBCD1) had a significant difference between F-AnGS and S-AnGS ($p < 0.05$, Fig. S5), but their total relative abundance was <0.2 %.

Moreover, the absolute abundance of functional genes involved in the anammox (*hzs*B) and denitrification (*nap*A, *nar*G, *nir*S, *nir*K, *nos*Z) pathway was quantified. The results showed that no significant difference of 16S rRNA gene was detected between F-AnGS and S-AnGS, indicating the same amount of microorganisms existed in both floating and settling granules. The average abundance of *hzs*B gene in F-AnGS were significantly higher than S-AnGS ($(1.4 \pm 0.2) \times 10^9$ vs. $(6.1 \pm 0.7) \times 10^8$ copies/g, $p < 0.05$), which could explain the higher specific anammox activity detected in Fig. 2a. A higher abundance of denitrification functional genes was also detected in anammox granules (Fig. 5b). Interestingly, F-AnGS hold a higher abundance of *nap*A and *nar*G genes responsible for reducing nitrate to nitrite than S-AnGS ($(2.9 \pm 0.4) \times 10^9$ vs. $(1.6 \pm 0.0) \times 10^9$ copies/g, $p < 0.05$), while S-AnGS contained a higher abundance of *nir*K and *nir*S (nitrite reductase genes) ($(9.6 \pm 0.6) \times 10^9$ vs. $(5.8 \pm 0.1) \times 10^9$ copies/g, $p < 0.01$). The co-occurring of heterotrophic bacteria in the anammox community are crucial to maintain the activity and stability of the microaggregates (Chen et al., 2019; Keren et al., 2020). The heterotrophs have been demonstrated to be the pioneering colonizers for anammox biofilm formation and forge complex cross-feeding interactions with AnAOB (Lawson et al., 2017; Niederdorfer et al., 2021; Zhao et al., 2018). Heterotrophs could grow on both soluble microbial products and detritus produced by AnAOB, even with no external carbon source (Ni et al., 2012), while the nitrate produced by AnAOB could be reduced to nitrite by heterotrophs to replenish the anammox substrate (Speth et al., 2016). By dosing folate to attenuate the cross-feeding between AnAOB and heterotrophs, the granule floatation could be efficiently alleviated (Xu et al., 2024). Overall, the variation of abundance of functional genes demonstrated the enhanced metabolic interaction between anammox bacteria and heterotrophs via the nitrite loop, which can further facilitate the granule floatation.

2.6. New insights into floatation mechanism of anammox granules

Anammox bacteria usually live in a communal lifestyle, and tend to form microbial aggregation, such as the granular sludge. Comparing to the conventional flocculated sludge, granular sludge has the advantages of space saving, higher removal rate, and greater resilience in practical wastewater engineering. However, the high-rate anammox granular system always face the great challenge of sludge floatation, which could deteriorate the nitrogen removal performance and washout the slow-growing anammox bacteria. The sludge flotation phenomenon is a dynamic equilibrium process. In the reactor, some settling granules could transition into the flotation state over time; while some floating granules settle back into the bottom zone, and others could be washed out with the effluent.

Previous studies hypothesize that the floatation of anammox granules was mainly caused by over-secreted EPS, which could block the gas-liquid channels, restrict the release of produced nitrogen gas, increase the whole density, and finally cause the granule floatation. In this study, we provide the direct evidence to quantify the gas entrapment in the floating granules, visualize their EPS distribution, and perform comparative analysis of microbial communities between the floating

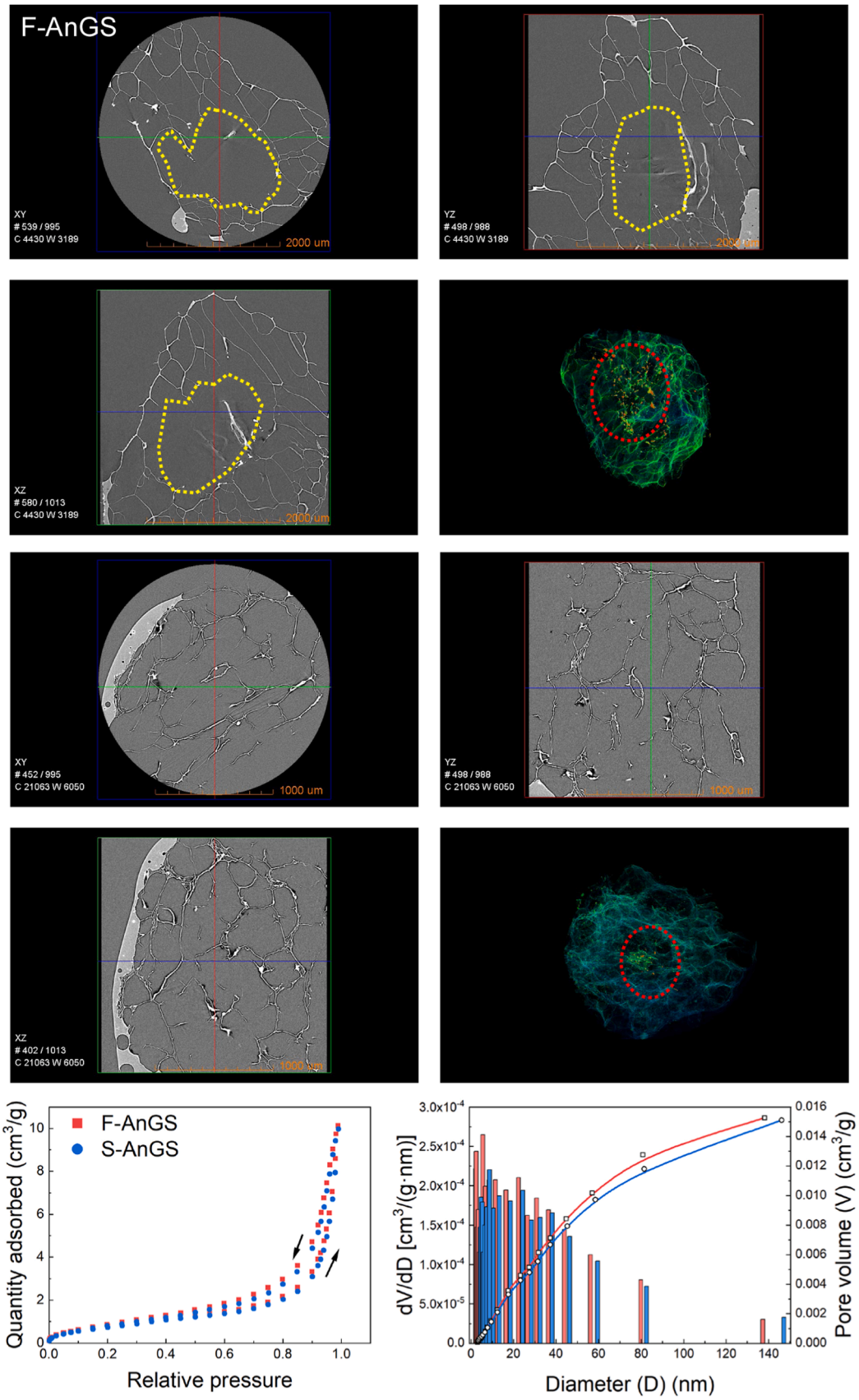

Fig. 4. 3D X-ray imaging of microstructure of the single F-AnGS (a), S-AnGS (b), and pore microstructure analysis (c) (both the different cross-sectional views and the 3D reconstruction view were displayed; the yellow circles represent the closed aera with no EPS penetration; while the red circles show the distribution of microbial aggregates).

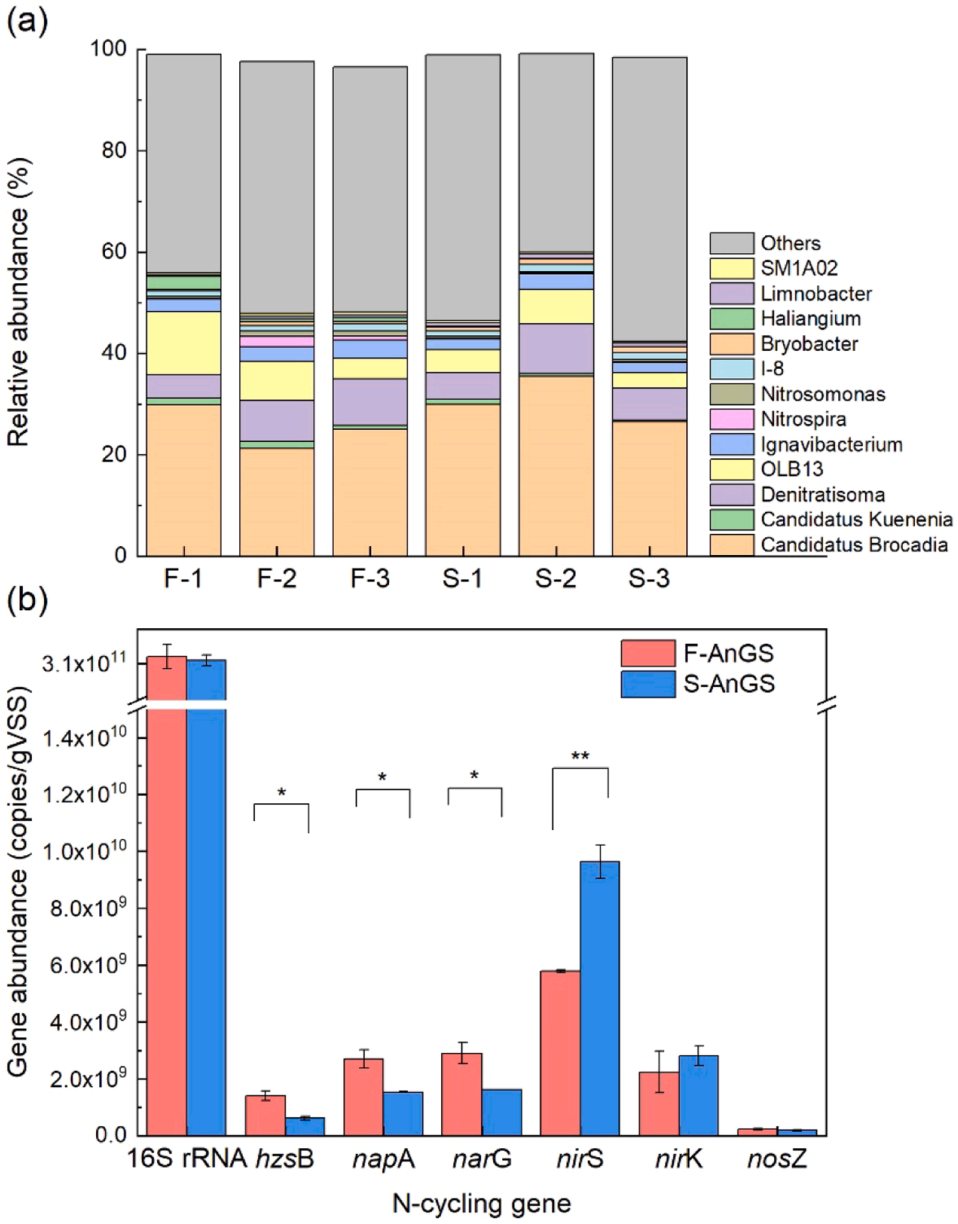

Fig. 5. (a) Relative abundance of microbial community at the genus level (three replicates each for F-AnGS and S-AnGS); (b) Absolute abundance of functional genes involved in the anammox and denitrification pathway.

and settling granules. To verify and deepen the previous hypothesis, the new insights into floatation mechanism of anammox granules we proposed in this study were shown in Fig. 6. Anammox granules can shift between the settling and floating states. The activity heterogeneity has been reported in the anammox granular system at the single granule level (Li et al., 2024). As the nitrogen load on the single granule increases, its specific activity will rise. Within the granule, in addition to the increase of total amount of EPS, we observed the heterogeneous distribution of EPS channels. Unlike the random distribution across different layer depth in the settling granules, EPS primarily distribute on the surface layer of the floating granule and form a closed area inside. This heterogeneous distribution will not only decrease the pore size, limit the gas escape, but also reduce the distance between microorganisms. Although the abundance of whole microbial community including the anammox bacteria did not increase significantly, the functional genes related to anammox and partial denitrification pathway increased, indicating the enhanced metabolic interaction between anammox bacteria and heterotrophs, which would further promote the activity. Both the over-excretion of EPS concentrated on the surface layer and enhanced microbial activity for nitrogen removal could contribute to gas accumulation within granules and finally lead to sludge floatation. When the high-rate granule floats to the water surface from the bottom to the top of the reactor, the limited substrate and dense surface of the floating granule will largely decrease its activity. With the decline of EPS excretion, the entrapped gas will disappear, and the floating granule will shift back to the settling state.

Based on our findings, the feasible strategies to alleviate the flotation of anammox granules include nitrogen load control, reactor design optimization, and microbial selection. Both substrate and biomass concentrations directly influence the nitrogen load on individual cells, subsequently affecting their aggregation and flotation behavior. However, the critical threshold of microbial nitrogen load distinguishing between settling and floating states remains unclear. Considering the significant heterogeneity among granules, further research focusing on tracking single-granule dynamics is needed to address this gap. Improving reactor mixing can alleviate flotation by enhancing gas-

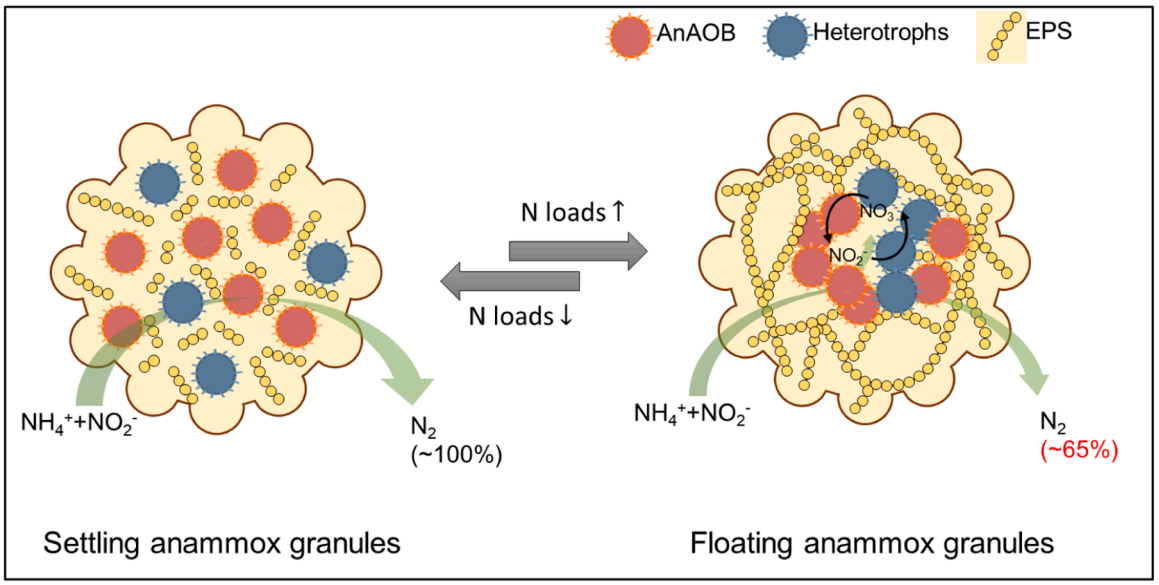

Fig. 6. Proposed mechanism for anammox granules shifting between the settling and floating states.

liquid-solid separation; however, it is crucial to balance this with the risk of structural disruption and biomass washout to ensure system stability. Microbial selection is an inherent and effective strategy to optimize the microstructure of anammox granules. However, understanding the EPS secretion capabilities of different species within the anammox community remains challenging. Further research combining metagenomics and culturomics is required to gain deeper insights into the ecophysiology of these species, facilitating more effective microbial selection and optimization of anammox granule microstructure.

3. Conclusions

This study reveals the floatation mechanism of anammox granules by comparing the structural and microbial characteristics with the settling granules. The following conclusions can be drawn:

1) The specific anammox activity of floating granules was 1.6 times higher than the settling granules, but only 65 % produced gas could be successfully released from the floating granules.
2) In addition to EPS accumulation, the heterogenous distribution of EPS, which forms a dense surface layer, was the main cause for granule floatation.
3) The enhanced metabolic interaction between anammox bacteria and heterotrophs via the nitrite loop further facilitated the granule floatation.

4. Materials and methods

4.1. Anammox granular system

A lab-scale upflow anaerobic sludge blanket (UASB) reactor was used in this study with the working volume of 1.5 L (Fig. S1). The inoculated anammox granular sludge was sampled from a pilot plant treating high ammonium-containing wastewater. The reactor was continually fed with synthetic medium containing 0.1 g N/L $(NH_4)_2SO_4$, 0.12 g N/L $NaNO_2$, 0.3 g/L $MgSO_4{\cdot}7H_2O$, 0.24 g/L $KHCO_3$, 0.4 g/L $NaHCO_3$, 0.0175 g/L KH_2PO_4, 0.0175 g/L $CaCl_2$ and 1.0 mL/L trace elements solutions (van de Graaf et al., 1996). The hydraulic retention time (HRT) was set at 3 h and the nitrogen loading rate (NLR) of anammox reactor was 1.8 kg N/(m^3·d). The anammox reactor maintained a stable and efficient nitrogen removal performance during this study (Table S1). The floating and settling anammox granules (F-AnGS and S-AnGS) were respectively collected from the top and bottom of the reactor on day 200 as shown in Fig. 1d.

4.2. Batch anammox activity tests

The batch anammox activity tests were performed according to the recommended manual (van Loosdrecht et al., 2016). The anammox granules were withdrawn from the reactor and washed using the nitrogen-free macro-nutrient solutions same as the reactor influent. Both F-AnGS and S-AnGS group was set in triplicates. 5 g anammox granules were added into the 100 mL serum bottle with 80 mL nitrogen-free macro-nutrient solutions. N_2 was sparged into the headspace for approximately 10 mins to ensure an oxygen-free environment and the serum bottles were sealed with butyl rubber stoppers and aluminum caps. The bottles were placed in a thermostatic shaker at 150 rpm and 30 °C. After the pre-incubation for approximately 30 min, the ammonium and nitrite were dosed into the bottles to reach final concentrations of 25 mg N/L. The mixed sludge liquor samples were collected every 1 h, filtered through 0.45 μm filter, and the concentrations of ammonium, nitrite, and nitrate were determined. The final MLVSS concentration (X_{VSS}) was determined for each group. The linear regression was used to determine the ammonium ($r_{AMX,NH4}$) and nitrite removal rates ($r_{AMX,NO2}$) as well as the nitrate production rate ($r_{AMX,NO3}$). The maximum specific anammox activity (r_{AMX}, expressed as mg N/(g VSS·d)) can be computed as $r_{AMX} = (r_{AMX,NH4} + r_{AMX,NO2} - r_{AMX,NO3})/X_{VSS}$.

4.3. Gas release determination

The anaerobic respirometry method was applied to measure the gas production rate and volume of anammox granules (Logan et al., 2002). The 250 mL vessels containing 7.5 g different granules (S-AnGS, F-AnGS and F-AnGS after vacuum degassing) were placed in a 30 °C water bath. The flow volume and rate of bubbles were automatically monitored and recorded every 10 mins by an AER-800 respirometer (Challenge Technology, USA). The initial concentrations of ammonium and nitrite were set as 50 mg N/L, after the gas release curves levelled off (at the time substrates were completely consumed), the concentrated substrates were reinjected to recover the initial concentrations, and three consecutive batch cycles were monitored for each group.

4.4. Physical analyses of anammox granules

The particle size distribution of anammox granules were determined by a laser particle size analyzer (Microtrac S3500, USA). ~3 ml sludge samples were prepared and the final results were averaged after three measurements. The Volume Mean Diameter (VMD) was adopted to represent the average size of anammox granules.

The pore analysis of the granules was measured using BET (Brunauer-Emmett-Teller) analysis, which is based on nitrogen gas adsorption. Prior to the analysis, the granules were freeze-dried to remove moisture while preserving their structural integrity. The dried samples were determined using an automated gas sorption analyzer (Autosorb iQ, Quantachrome, USA). Nitrogen adsorption-desorption isotherms were recorded at liquid nitrogen temperature (−196 °C). The specific surface area was calculated using the BET equation over a relative pressure range of 0–1. Total pore volume was determined from the amount of nitrogen adsorbed at a relative pressure close to 1, assuming the pores were completely filled with liquid nitrogen. The pore size distribution was calculated using the Barrett-Joyner-Halenda (BJH) method by analyzing the adsorption branch of the nitrogen adsorption-desorption isotherm (Bardestani et al., 2019). The derivative dV/dD, representing the change in pore volume (V) with respect to pore diameter (D), is computed to generate a detailed pore size distribution (PSD) curve.

4.5. EPS analysis and imaging

The extracellular polymeric substances (EPS) were extracted using a modified heat extraction method (Li and Yang, 2007) and three sub-fractions of EPS, slime (S), loosely bound EPS (LB) and tightly bound EPS (TB) were respectively obtained. Each sample were prepared with three replicates. The content of EPS was firstly characterized with colorimetric methods. For each stratified EPS, the protein (PN) and polysaccharide (PS) were respectively quantified using the modified Lowry method with bovine serum albumin as the standard (Frølund et al., 1996), and the phenol sulfuric acid method with glucose as the standard (DuBois et al., 1956).

In addition, the characterization of fluorescence components within the EPS was conducted using the three-dimensional excitation-emission (3D-EEM) matrix. The stratified EPS was determined by a fluorescence spectrophotometer (Hitachi F7100, Japan). The range of excitation spectra was set from 200 to 400 nm at 10 nm increments and emission spectra from 200 to 500 nm at 5 nm increments. The scanning speed was set at 12,000 nm/min. The spectra of individual samples were further processed using R package staRdom (v1.1.28) (Pucher, 2020). Deionized water served as the blank and was subtracted from the spectra, all the spectra data were normalized using Raman normalization method and both the Raman and Rayleigh scattering were removed. The peaks were listed in Table S3.

To visualize the microstructure, particularly the EPS distribution within the granule, single floating and settling granules were randomly selected and scanned using a 3D X-ray microscope (XRM) (ZEISS Xradia 520 Versa, Germany). Each granule was mounted on a holder using a centrifuge tube as an adapter and rotated horizontally by 180° to collect 2D projection images at discrete angles. The scanning energies were set to vary between 30 and 160 kV. Image stacks of about 1000 virtual slices with 3.5 μm voxel sizes were acquired on XRM, which were then combined together to produce a 3D reconstruction of the volume dataset. The 3D imaging result was reviewed and colored with XRMViewer software.

4.6. 16S rRNA gene sequencing

The genomic DNA of F-AnGS and S-AnGS sampled at day 200 was respectively extracted using the FastDNA Spin kit for Soil (MP Biomedicals, USA) according to the manufacturer's instructions. Both F-AnGS and S-AnGS group had three replicates. The quantity of DNA was checked with a NanoDrop spectrophotometer (Thermo Fisher Scientific, USA). Each sample was amplified using specific primers (338F and 806R) with a barcode targeting the V3-V4 region of 16S rRNA gene. The amplicons were checked, pooled, purified and sequenced on the Illumina Novaseq 6000 platform (Illumina Inc., San Diego, CA, USA) by Guangdong Magigene Biotechnology Co., Ltd. (Guangzhou, China). Pair-end raw reads with maximum read length of 250 bp were quality controlled by fastp (v0.14.1) (Chen et al., 2018) and then merged by usearch (v10.0.240) (Edgar, 2010). The advanced DADA2 algorithms within Qiime2 (v2020.11.0) pipelines was applied to denoise, correct errors and remove chimeras to obtain the amplicon sequence variants (ASVs) (Bolyen et al., 2019; Callahan et al., 2016). ASVs with fewer than 20 reads (<0.03 %) were filtered out and taxonomy assignment was performed based on the SILVA reference database (v132) (Quast et al., 2012). Detailed sequencing information was summarized in Table S2. The raw reads have been deposited to the Sequence Read Archive (SRA) database of NCBI under the accession number of PRJNA1060873.

4.7. Real-time PCR

A high-throughput qPCR chip was used in SmartChip Real-Time PCR System (WaferGen Biosystems USA) was used to quantify the absolute abundance of nitrogen-cycling functional genes (Zheng et al., 2018). The hydrazine synthase genes (*hzs*B) were chosen as the qPCR primers for anammox bacteria detection with high specificity (Zhou et al., 2018), while *nar*G/*nap*A, *nir*S/*nir*K, *nos*Z genes were used to quantify the denitrifying bacteria. Detailed information for the primers were listed in Table S4. The amplification efficiency was quality controlled between 1.8 and 2.2, and the absolute abundance of each target gene was calculated according to the absolute quantitative conversion of 16S rRNA gene following the formula: 16S rRNA gene relative quantification/16S rRNA gene absolute quantification = Target gene relative quantification/Target gene absolute quantification.

4.8. Regular analyses

The bulk concentrations of NH_4^+, NO_2^-, and NO_3^- were determined by Quikchem 8500 flow injection analysis system (HACH, USA) after filtering into 0.45 μm filter. The mixed liquor volatile suspended solid (MLVSS) was determined by the prepASH 340 thermogravimetric analyzer (Precisa, Switzerland). The statistical difference between two groups of F-AnGS and S-AnGS were assessed using student *t*-test, where $p < 0.05$ has significance (*) and $p < 0.01$ has high significance (**).

CRediT authorship contribution statement

Da Kang: Writing – original draft, Formal analysis, Conceptualization. **Huifeng Lu:** Investigation, Data curation. **Tingting Kang:** Methodology, Investigation. **Yihan Zhang:** Formal analysis. **Zheng Ge:** Methodology. **Liang Zhang:** Writing – review & editing. **Yongzhen Peng:** Supervision.

Declaration of competing interest

The authors declare that they have no known competing financial interests or personal relationships that could have appeared to influence the work reported in this paper.

Acknowledgment

This research was financially supported by the National Natural Science Foundation of China (52200032 and U23A20675).

Supplementary materials

Supplementary material associated with this article can be found, in the online version, at doi:10.1016/j.wroa.2025.100319.

Data availability

Data will be made available on request

References

Abma, W.R., Schultz, C.E., Mulder, J.W., van der Star, W.R., Strous, M., Tokutomi, T., van Loosdrecht, M.C., 2007. Full-scale granular sludge Anammox process. Water Sci. Technol. 55 (8–9), 27–33.

Adams, M., Xie, J.X., Kabore, A.W.J., Chang, Y.F., Xie, J.W., Guo, M.L., Chen, C.J., 2022. Research advances in anammox granular sludge: a review. Crit. Rev. Environ. Sci. Technol. 52 (5), 631–674.

Ali, M., Shaw, D.R., Zhang, L., Haroon, M.F., Narita, Y., Emwas, A.H., Saikaly, P.E., Okabe, S., 2018. Aggregation ability of three phylogenetically distant anammox bacterial species. Water Res 143, 10–18.

Bardestani, R., Patience, G.S., Kaliaguine, S., 2019. Experimental methods in chemical engineering: specific surface area and pore size distribution measurements-BET, BJH, and DFT. Can. J. Chem. En.g 97 (11), 2781–2791.

Bolyen, E., Rideout, J.R., Dillon, M.R., Bokulich, N.A., Abnet, C.C., Al-Ghalith, G.A., Alexander, H., Alm, E.J., Arumugam, M., Asnicar, F., 2019. Reproducible, interactive, scalable and extensible microbiome data science using QIIME 2. Nat. Biotechnol. 37 (8), 852–857.

Callahan, B.J., McMurdie, P.J., Rosen, M.J., Han, A.W., Johnson, A.J.A., Holmes, S.P., 2016. DADA2: high-resolution sample inference from Illumina amplicon data. Nat. Methods 13 (7), 581–583.

Cao, Y., van Loosdrecht, M.C., Daigger, G.T., 2017. Mainstream partial nitritation-anammox in municipal wastewater treatment: status, bottlenecks, and further studies. Appl. Microbiol. Biotechnol. 101 (4), 1365–1383.

Chen, J., Ji, Q., Zheng, P., Chen, T., Wang, C., Mahmood, Q., 2010. Floatation and control of granular sludge in a high-rate anammox reactor. Water Res 44 (11), 3321–3328.

Chen, S., Zhou, Y., Chen, Y., Gu, J., 2018. fastp: an ultra-fast all-in-one FASTQ preprocessor. Bioinformatics 34 (17), i884–i890.

Chen, W., Westerhoff, P., Leenheer, J.A., Booksh, K., 2003. Fluorescence excitation–emission matrix regional integration to quantify spectra for dissolved organic matter. Environ. Sci. Technol. 37 (24), 5701–5710.

Chen, Z., Meng, Y., Sheng, B., Zhou, Z., Jin, C., Meng, F., 2019. Linking exoproteome function and structure to anammox biofilm development. Environ. Sci. Technol. 53 (3), 1490–1500.

Dapena-Mora, A., Fernandez, I., Campos, J.L., Mosquera-Corral, A., Mendez, R., Jetten, M.S.M., 2007. Evaluation of activity and inhibition effects on Anammox process by batch tests based on the nitrogen gas production. Enzyme Microb. Technol. 40 (4), 859–865.

DuBois, M., Gilles, K.A., Hamilton, J.K., Rebers, P.A., Smith, F., 1956. Colorimetric method for determination of sugars and related substances. Anal. Chem. 28 (3), 350–356.

Edgar, R.C., 2010. Search and clustering orders of magnitude faster than BLAST. Bioinformatics 26 (19), 2460–2461.

Flemming, H.C., Wingender, J., 2010. The biofilm matrix. Nat. Rev. Microbiol. 8 (9), 623–633.

Frølund, B., Palmgren, R., Keiding, K., Nielsen, P.H., 1996. Extraction of extracellular polymers from activated sludge using a cation exchange resin. Water Res 30 (8), 1749–1758.

Fu, H.-M., Peng, M.-W., Yan, P., Wei, Z., Fang, F., Guo, J.-S., Chen, Y.-P., 2021. Potential role of nanobubbles in dynamically modulating the structure and stability of anammox granular sludge within biological nitrogen removal process. Sci. Total Environ. 784, 147110.

Gregg, S.J., Sing, K.S.W., Salzberg, H., 1967. Adsorption surface area and porosity. J. Electrochem. Soc. 114 (11), 279Ca.

Hou, X., Liu, S., Zhang, Z., 2015. Role of extracellular polymeric substance in determining the high aggregation ability of anammox sludge. Water Res 75, 51–62.

Jia, F.X., Yang, Q., Liu, X.H., Li, X.Y., Li, B.K., Zhang, L., Peng, Y.Z., 2017. Stratification of extracellular polymeric substances (EPS) for aggregated anammox microorganisms. Environ. Sci. Technol. 51 (6), 3260–3268.

Jin, R.C., Yang, G.F., Yu, J.J., Zheng, P., 2012. The inhibition of the Anammox process: a review. Chem. Eng. J. 197, 67–79.

Keren, R., Lawrence, J.E., Zhuang, W.Q., Jenkins, D., Banfield, J.F., Alvarez-Cohen, L., Zhou, L.J., Yu, K., 2020. Increased replication of dissimilatory nitrate-reducing bacteria leads to decreased anammox bioreactor performance. Microbiome 8 (1).

Kosgey, K., Chandran, K., Gokal, J., Kiambi, S.L., Bux, F., Kumari, S., 2021. Critical analysis of biomass retention strategies in mainstream and sidestream ANAMMOX-mediated nitrogen Removal systems. Environ. Sci. Technol. 55 (1), 9–24.

Kuenen, J.G., 2020. Anammox and beyond. Environ. Microbiol. 22 (2), 525–536.

Lackner, S., Gilbert, E.M., Vlaeminck, S.E., Joss, A., Horn, H., van Loosdrecht, M.C., 2014. Full-scale partial nitritation/anammox experiences-an application survey. Water Res 55, 292–303.

Lawson, C.E., Wu, S., Bhattacharjee, A.S., Hamilton, J.J., McMahon, K.D., Goel, R., Noguera, D.R., 2017. Metabolic network analysis reveals microbial community interactions in anammox granules. Nat. Commun. 8, 12.

Li, S.-J., Li, H., Fu, H.-M., Weng, X., Zhu, Z., Wang, W., Chen, Y.-P., 2024. Monitoring the biochemical activity of single anammox granules with microbarometers. Environ. Sci. Technol.

Li, X.Y., Yang, S.F., 2007. Influence of loosely bound extracellular polymeric substances (EPS) on the flocculation, sedimentation and dewaterability of activated sludge. Water Res 41 (5), 1022–1030.

Logan, B.E., Oh, S.-E., Kim, I.S., Van Ginkel, S., 2002. Biological hydrogen production measured in batch anaerobic respirometers. Environ. Sci. Technol. 36 (11), 2530–2535.

Lotti, T., Kleerebezem, R., Lubello, C., van Loosdrecht, M.C.M., 2014. Physiological and kinetic characterization of a suspended cell anammox culture. Water Res 60, 1–14.

Lu, H.F., Ji, Q.X., Ding, S., Zheng, P., 2013. The morphological and settling properties of ANAMMOX granular sludge in high-rate reactors. Bioresour. Technol. 143, 592–597.

Lu, H.F., Zheng, P., Ji, Q.X., Zhang, H.T., Ji, J.Y., Wang, L., Ding, S., Chen, T.T., Zhang, J. Q., Tang, C.J., Chen, J.W., 2012. The structure, density and settlability of anammox granular sludge in high-rate reactors. Bioresour. Technol. 123, 312–317.

Ma, J., Yang, W., Ke, S., He, Q., Zhao, Q., Yin, H., 2023. Microbial community dynamics and performance of simultaneous anammox and denitrification (SAD) process at varying substrate loadings during long-term operation. J. Environ. Chem. Eng. 11 (3), 110225.

McCarty, P.L., 2018. What is the best biological process for nitrogen removal: when and why? Environ. Sci. Technol. 52 (7), 3835–3841.

Ni, B.J., Chen, Y.P., Liu, S.Y., Fang, F., Xie, W.M., Yu, H.Q., 2009. Modeling a granule-based Anaerobic ammonium oxidizing (ANAMMOX) process. Biotechnol. Bioeng. 103 (3), 490–499.

Ni, B.J., Ruscalleda, M., Smets, B.F., 2012. Evaluation on the microbial interactions of anaerobic ammonium oxidizers and heterotrophs in Anammox biofilm. Water Res 46 (15), 4645–4652.

Niederdorfer, R., Fragner, L., Yuan, L., Hausherr, D., Wei, J., Magyar, P., Joss, A., Lehmann, M.F., Ju, F., Bürgmann, H., 2021. Distinct growth stages controlled by the interplay of deterministic and stochastic processes in functional anammox biofilms. Water Res 200, 117225.

Oshiki, M., Hiraizumi, H., Satoh, H., Okabe, S., 2020. Cell density-dependent anammox activity of Candidatus Brocadia sinica regulated by N-acyl homoserine lactone-mediated quorum sensing. Microb. Environ. 35 (4), ME20086.

Oshiki, M., Satoh, H., Okabe, S., 2016. Ecology and physiology of anaerobic ammonium oxidizing bacteria. Environ. Microbiol. 18 (9), 2784–2796.

Pucher, M., 2020. PARAFAC analysis of EEM data to separate DOM components in R. staRdom: spectroscopic analysis of dissolved organic matter in R. Retrieved from https://cran.r-project.org/web/packages/staRdom/vignettes/PARAFAC_analysis_of_EEM.html.

Quast, C., Pruesse, E., Yilmaz, P., Gerken, J., Schweer, T., Yarza, P., Peplies, J., Glöckner, F.O., 2012. The SILVA ribosomal RNA gene database project: improved data processing and web-based tools. Nucl. Acids Res 41 (D1), D590–D596.

Song, Y.X., Liao, Q., Yu, C., Xiao, R.Y., Tang, C.J., Chai, L.Y., Duan, C.S., 2017. Physicochemical and microbial properties of settled and floating anammox granules in upflow reactor. Biochem. Eng. J. 123, 75–85.

Speth, D.R., Guerrero-Cruz, S., Dutilh, B.E., Jetten, M.S., 2016. Genome-based microbial ecology of anammox granules in a full-scale wastewater treatment system. Nat. Commun. 7, 11172.

Strous, M., Heijnen, J., Kuenen, J.G., Jetten, M., 1998. The sequencing batch reactor as a powerful tool for the study of slowly growing anaerobic ammonium-oxidizing microorganisms. Appl. Microbiol. Biotechnol. 50 (5), 589–596.

Tan, H., Wang, Y., Tang, X., Li, L., Feng, F., Mahmood, Q., Wu, D., Tang, C.-J., 2020. Quantitative determination of cavitation formation and sludge flotation in Anammox granules by using a new diffusion-reaction integrated mathematical model. Water Res, 115632.

Tang, C.J., Zheng, P., Wang, C.H., Mahmood, Q., Zhang, J.Q., Chen, X.G., Zhang, L., Chen, J.W., 2011. Performance of high-loaded ANAMMOX UASB reactors containing granular sludge. Water Res 45 (1), 135–144.

Tao, J., Xing, J., Wang, D., Sheng, B., Meng, F., 2020. Deciphering the genesis of anammox granular sludge floating from the perspective of microbial community. J. Water Process Eng. 36, 101265.

van de Graaf, A.A., de Bruijn, P., Robertson, L.A., Jetten, M.S., Kuenen, J.G., 1996. Autotrophic growth of anaerobic ammonium-oxidizing micro-organisms in a fluidized bed reactor. Microbiology 142 (8), 2187–2196.

van der Star, W.R.L., Abma, W.R., Blommers, D., Mulder, J.W., Tokutomi, T., Strous, M., Picioreanu, C., Van Loosdrecht, M.C.M., 2007. Startup of reactors for anoxic ammonium oxidation: experiences from the first full-scale anammox reactor in Rotterdam. Water Res 41 (18), 4149–4163.

van Loosdrecht, M.C., Nielsen, P.H., Lopez-Vazquez, C.M., Brdjanovic, D., 2016. Experimental Methods in Wastewater Treatment. IWA publishing.

Winkler, M.K.H., Meunier, C., Henriet, O., Mahillon, J., Suarez-Ojeda, M.E., Del Moro, G., De Sanctis, M., Di Iaconi, C., Weissbrodt, D.G., 2018. An integrative review of granular sludge for the biological removal of nutrients and recalcitrant organic matter from wastewater. Chem. Eng. J. 336, 489–502.

Xiao, R., Zheng, Y., 2016. Overview of microalgal extracellular polymeric substances (EPS) and their applications. Biotechnol. Adv. 34 (7), 1225–1244.

Xiao, R., Zhu, W., Zheng, Y., Xu, S., Lu, H., 2022. Active assimilators of soluble microbial products produced by wastewater anammox bacteria and their roles revealed by DNA-SIP coupled to metagenomics. Environ. Int., 107265

Xu, D., Fan, J., Li, W., Chen, W., Pan, C., Kang, D., Li, Y., Shan, S., Zheng, P., 2021. Deciphering correlation between permeability and size of anammox granule: "pores as medium. Water Res 191, 116832.
Xu, D., Pan, C., Liu, S., Guo, J., Zheng, P., Zhang, M., 2024. Efficient alleviation granular sludge floatation in a high-rate anammox reactor by dosing folate. Water Res 264, 122249.
Xue, Y., Ma, H., Li, Y.-Y., 2023. Anammox-based granulation cycle for sustainable granular sludge biotechnology from mechanisms to strategies: a critical review. Water Res 228, 119353.
Yu, J., Xiao, K., Xu, H., Li, Y., Xue, Q., Xue, W., Zhang, A., Wen, X., Xu, G., Huang, X., 2023. Spectroscopic fingerprints profiling the polysaccharide/protein/humic architecture of stratified extracellular polymeric substances (EPS) in activated sludge. Water Res 235, 119866.
Zhao, Y.P., Liu, S.F., Jiang, B., Feng, Y., Zhu, T.T., Tao, H.C., Tang, X., Liu, S.T., 2018. Genome-centered metagenomics analysis reveals the symbiotic organisms possessing ability to cross-feed with anammox bacteria in anammox consortia. Environ. Sci. Technol. 52 (19), 11285–11296.
Zheng, B., Zhu, Y., Sardans, J., Peñuelas, J., Su, J., 2018. QMEC: a tool for high-throughput quantitative assessment of microbial functional potential in C, N, P, and S biogeochemical cycling. Sci. China Life Sci. 61, 1451–1462.
Zhou, Y., Wang, C., Xu, X., Jin, W., Liu, L., Meng, F., Yang, F., 2023. Deciphering the partial denitrification function of companion bacteria in mixotrophic anammox systems under different carbon/nitrogen ratios. J. Environ. Chem. Eng. 11 (6), 111232.
Zhou, Z.C., Wei, Q.Y., Yang, Y.C., Li, M., Gu, J.D., 2018. Practical applications of PCR primers in detection of anammox bacteria effectively from different types of samples. Appl. Microbiol. Biotechnol. 102 (14), 5859–5871.
Zhu, G., Wang, S., Ma, B., Wang, X., Zhou, J., Zhao, S., Liu, R., 2018. Anammox granular sludge in low-ammonium sewage treatment: not bigger size driving better performance. Water Res 142, 147–158.